

# Chiroptical hot spots in twisted nanowire plasmonic oscillators

Yiqiao Tang, Li Sun, Adam E. Cohen<sup>1</sup>

## Supporting information

### Supporting Information:

1. Nanofabrication
2. Spectroscopic polarizing microscope
3. Single-wire linear dichroism and linear birefringence
4. Data acquisition and analysis
5. Analytical calculation of dissymmetry factor

### 1. Nanofabrication

Gold nanowires were fabricated using electron-beam lithography following standard procedures. Briefly, clean fused silica coverslips were coated with poly(methyl methacrylate) (PMMA, molecular weight 495,000) via spin coating (40 s at 4000 rpm). Samples were baked at 180 °C for 10 min. Another layer of PMMA (molecular weight 950,000) was deposited over the first layer via spin coating (40 s at 4000 rpm). The sample was baked again at 180 °C for 10 min, and then coated with a water-soluble conducting polymer (Showa Denko, Espacer 300; 30 s at 2000 rpm). The conductive layer was necessary to prevent sample charging during the e-beam writing process.

---

<sup>1</sup> to whom correspondence should be addressed: [cohen@chemistry.harvard.edu](mailto:cohen@chemistry.harvard.edu)

Lithography was performed on a Raith 150. Samples were developed in 1:3 MIBK:IPA for 40 s, yielding wire-shaped grooves in the PMMA. Metal was deposited via thermal evaporation (1.5 nm Ti adhesion layer, 30 nm Au). Liftoff was performed in acetone overnight. The nanowires were 100 nm in width, 20  $\mu\text{m}$  in length and 30 nm in thickness. The spacing between adjacent wires was 5  $\mu\text{m}$ .

## **2. Spectroscopic polarizing microscope**

Light from a tungsten-halogen lamp (Ocean Optics HL-2000) passed through a homemade Czerny-Turner monochromator. The monochromator consisted of two silver-coated concave mirrors ( $f = 100$  mm: Thorlabs CM508-100-P01), a ruled diffraction grating (Thorlabs GR50-1210; 1200 lines/mm, blazed for 1  $\mu\text{m}$ ) and adjustable mechanical entrance and exit slits (Thorlabs VA100). The diffraction grating was mounted on a motorized rotation stage (Thorlabs PRM1Z8), to facilitate wavelength scanning.

The light passed through a focusing lens ( $f = 80$  mm: Thorlabs, AC508-080-B-ML) before a linear polarizer, selected for good transmission and high contrast in the visible and NIR (Codixx colorPol VIS-IR). The polarizer was mounted on a motorized rotation stage (Thorlabs PRM1Z8). A liquid crystal variable retarder (Meadowlark, LRC-200-IR1-1L) allowed rapid (< 30 ms) switching of the polarization between left circular, right circular, linear horizontal or linear vertical. Rapid switching was essential to achieve sufficient sensitivity for circular dichroism measurements. We found that to achieve high quality CPL, it was necessary to adjust the angle of the polarizer by up to  $3^\circ$  between left- and right-CPL. We took care to quantify and

correct for spurious linear birefringence or linear dichroism in any of the optical elements. All the measurements were performed under ellipticities  $> 99\%$  at the sample plane.

The CLIC geometry was formed by pressing down on the top substrate with an N-BK7 plano-convex lens ( $f = 100$  mm: Thorlabs, LA1207). To minimize stray reflections and to prevent scratches at the interface between the pushing lens and the top substrate, immersion oil (Cargille Labs, type FF) was applied at this interface. Images were collected by an objective lens (4 $\times$ : Olympus Plan 4x/0.1; 40 $\times$ : Olympus LCPlanFL 40x/0.60 Ph2). An 18 cm focal length tube lens (Olympus U-TLU-1-2) projected the image onto an EMCCD camera (Andor DU-897, 512 x 512 pixels), cooled to  $-70$  °C.

At the moment of physical contact between the coverslips, we observed slight damage to the nanowires at the contact point. We used this damage as an indicator of contact. Data was acquired in regions near the contact point where the nanowires remained intact. The upper limit on the gap height we measured was set by the requirement to keep both sets of nanowires in focus simultaneously.

### **3. Single-wire linear dichroism and linear birefringence**

Linear dichroism and linear birefringence were measured on a single plane of nanowires, with the top set of nanowires removed from the apparatus (Fig. S1). To measure linear dichroism, the LCVR was switched between zero- and half-wave retardance, leading to linearly polarized illumination either parallel or perpendicular to the nanowire axis. Transmitted light images were recorded on the EMCCD camera. We constructed linear dichroism maps in a manner analogous

to the construction of the circular dichroism maps. The measured linear dichroism spectrum (Fig. S2) was in quantitative agreement with earlier measurements on chemically synthesized Au nanorods<sup>1</sup>.

To measure linear birefringence, a second linear polarizer (Codixx colorPol VIS-IR) was placed between the objective and the tube lens, with transmission axis at 45° relative to the nanowire axis (Figure S3). The LCVR alternated between 1/4- and 3/4-wave retardance, creating alternately left- and right-CPL on the sample. Linear birefringence in the sample converted the polarization to elliptical, with major axis alternately parallel and perpendicular to the second polarizer. Images were acquired on the EMCCD camera. We constructed linear birefringence maps in a manner analogous to the construction of circular dichroism maps.

The linear birefringence measurement yielded the relative phase shift of scattered linearly polarized light in the parallel vs. perpendicular orientations. This measurement did not yield the phase shift of the scattered light relative to the incident light. We left this overall phase,  $\psi$ , as a fitting parameter. The other fitting parameter was the overall polarizability of each particle,  $A_0$ .

#### **4. Data acquisition and analysis**

In a typical data set, 40 images were acquired under alternating left- and right-CPL at each wavelength. Typical exposure times were 300 ms. The orientations of the optics and the LCVR control voltages were tuned manually to achieve maximal ellipticities (> 99%) at each wavelength. The apparatus was controlled by custom software written in LabView and analysis was performed in Matlab.

We found that the lamp exhibited small frame-to-frame fluctuations in intensity ( $< 1\%$ ), and that the transmission of the LCVR varied by  $\sim 1\%$  depending on the control voltage. To correct for these artifacts, we normalized each frame by the intensity in a nanowire-free region. We then averaged measurements taken under corresponding polarizations.

Circular dichroism dissymmetry maps were calculated according to:

$$g = \frac{2(I^L - I^R)}{I^L + I^R}$$

where  $I^L$  and  $I^R$  represent the images acquired under left- and right-CPL, respectively. The coordinates of nanowire crossings were determined by automated image processing.

Each high-magnification image was located within a low-magnification image of Newton's rings. The weak interference pattern visible within the high magnification image was used to calculate the gap height  $h$  at each nanowire junction. Dissymmetry images around junctions with similar values of  $h$  were grouped and averaged.

## 5. Analytical calculation of dissymmetry factor

We consider two identical anisotropic polarizable particles, located at  $\mathbf{r}_1 = (0,0,0)$  and  $\mathbf{r}_2 = (0,0,h)$ . The principal axes of the particles are  $\boldsymbol{\mu}_1 = \hat{\mathbf{x}}$  and  $\boldsymbol{\mu}_2 = \hat{\mathbf{x}} \cos \theta + \hat{\mathbf{y}} \sin \theta$ . The particles are exposed to circularly polarized illumination, with electric field  $\mathbf{E}^{(0)} = E_0(\hat{\mathbf{x}} \pm i\hat{\mathbf{y}})e^{i(kz - \omega t)}$ . This field propagates along  $\hat{\mathbf{z}}$ , with wave vector  $\mathbf{k}$  and angular frequency  $\omega$ . The + and - signs represent left- and right-circular polarization, respectively.

If we neglect dipole-dipole coupling, then the polarization of each particle is  $\mathbf{P}_i^{(0)} = \boldsymbol{\alpha}_i \cdot \mathbf{E}_i^{(0)}$ , where  $i = 1$  or  $2$ , and  $\boldsymbol{\alpha}_i$  is the frequency-dependent complex polarizability tensor. The single-rod polarizability is:

$$\boldsymbol{\alpha}_i = \varepsilon_0 AVR(\phi_i) \begin{pmatrix} 1 & 0 \\ 0 & \rho e^{i\beta} \end{pmatrix} R(-\phi_i), \quad (\text{S1})$$

where  $\rho$  and  $\beta$  measure linear dichroism and linear birefringence respectively, and the overall amplitude and phase of the particle response are determined by a complex coefficient  $A = A_0 e^{i\psi}$ . These four parameters ( $\rho$ ,  $\beta$ ,  $A_0$ , and  $\psi$ ) depend on the frequency of illumination, the composition of the particle, and its shape. The rotation matrix  $R(\phi_i)$  accounts for the orientation of the particles ( $\phi_1 = 0$ ,  $\phi_2 = \theta$ ).  $V$  is an effective volume for the particle.

To introduce enantioselection, we include coupling between the two dipoles. Oscillating dipole  $\mathbf{P}_j^{(0)}$  induces a first-order correction to the electric field  $\mathbf{E}_i^{(1)}$  at location  $\mathbf{r}_i$ , ( $i, j = 1, 2; i \neq j$ ). The electric field propagates according to the retarded Green's function:

$$\mathbf{E}_j^{(1)} = \boldsymbol{\Gamma}(\mathbf{r}_{ij}) \mathbf{P}_i^{(0)},$$

where

$$\boldsymbol{\Gamma}(\mathbf{r}) = (3\hat{\mathbf{r}}\hat{\mathbf{r}} - \mathbf{1}) \left( \frac{1}{r^2} - \frac{ik}{r} \right) \frac{e^{ikr}}{4\pi\varepsilon_0 r} + (\mathbf{1} - \hat{\mathbf{r}}\hat{\mathbf{r}}) \frac{k^2 e^{ikr}}{4\pi\varepsilon_0 r} - \frac{1}{3\varepsilon_0} \delta^3(\mathbf{r}). \quad (\text{S2})$$

In the first Born approximation we neglect higher-order couplings between the rods (i.e. multiple scattering events). We used the far-field limit of Eq. S2 which, for displacements along the  $z$ -axis, becomes

$$\Gamma_{ff}(z) = \frac{k^2 e^{ikz}}{4\pi\epsilon_0 z} \quad (\text{S3})$$

The total dipole  $\mathbf{P}_i$  becomes:

$$\mathbf{P}_i = \boldsymbol{\alpha}_i \cdot (\mathbf{E}_i^{(0)} + \mathbf{E}_i^{(1)}). \quad (\text{S4})$$

We consider a detector located at height  $z$  (assuming  $z \gg h$ ). The electric field at the detector is:

$$\mathbf{E}_d(z) = \Gamma_{ff}(z)\mathbf{P}_1 + \Gamma_{ff}(z-h)\mathbf{P}_2 + \mathbf{E}^{(0)}(z). \quad (\text{S5})$$

Eq. S5 is evaluated successively for left- and right CPL, to yield electric fields at the detector  $\mathbf{E}_d^+$  and  $\mathbf{E}_d^-$ . The measured dissymmetry factor,  $g$ , equals

$$g = \frac{2\left(|\mathbf{E}_d^+|^2 - |\mathbf{E}_d^-|^2\right)}{|\mathbf{E}_d^+|^2 + |\mathbf{E}_d^-|^2}. \quad (\text{S6})$$

## Supporting References

1. Al-Rawashdeh, N. A. F.; Sandrock, M. L.; Seugling, C. J.; Foss Jr, C. A. *The Journal of Physical Chemistry B* **1998**, 102, 361.

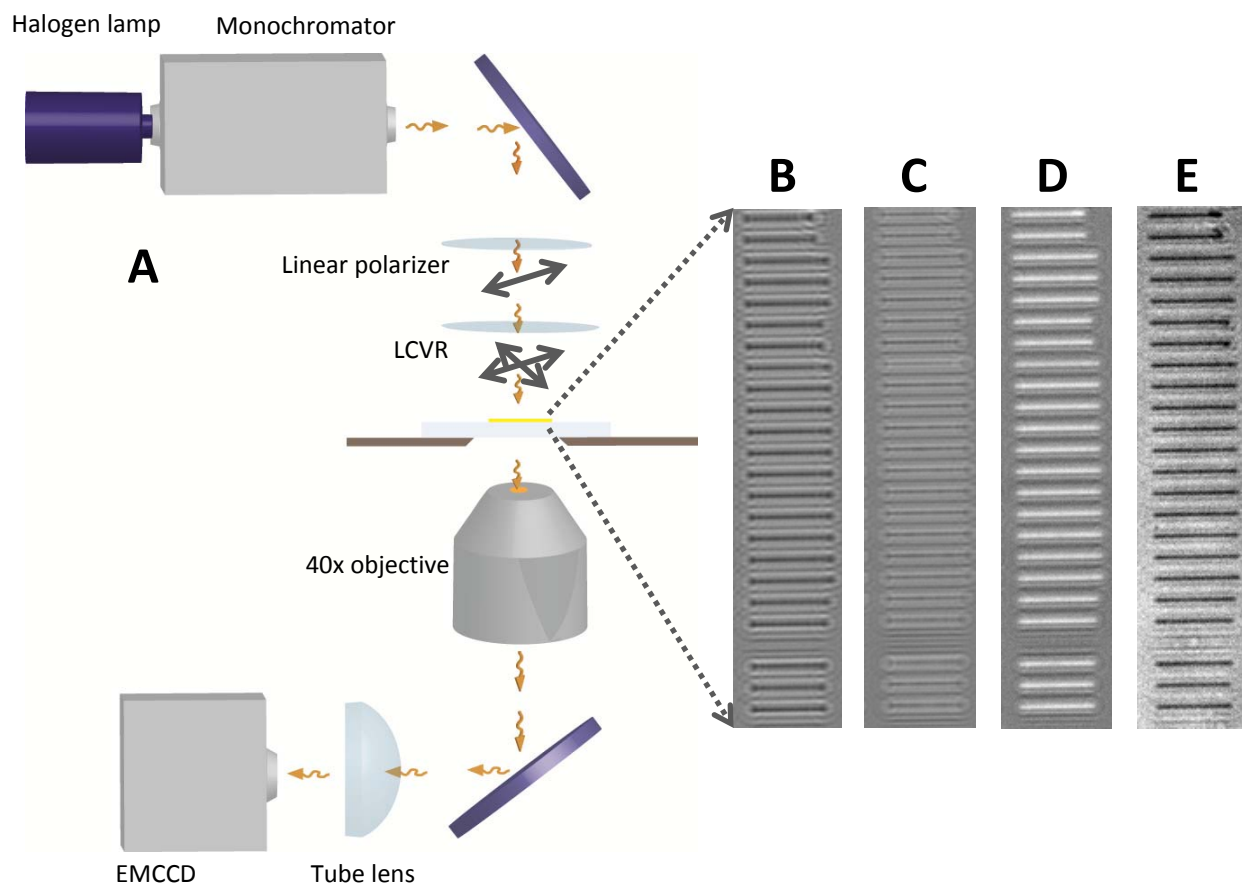


**Figure S1** Linear dichroism of single nanowires. A. Experimental apparatus. The LCVR controlled the incident polarization to be alternately parallel or perpendicular to the nanowire axes. Maps of linear dichroism at (B) 600 nm, (C) 630 nm (D) 760 nm. E. Photograph of nanowire arrays.



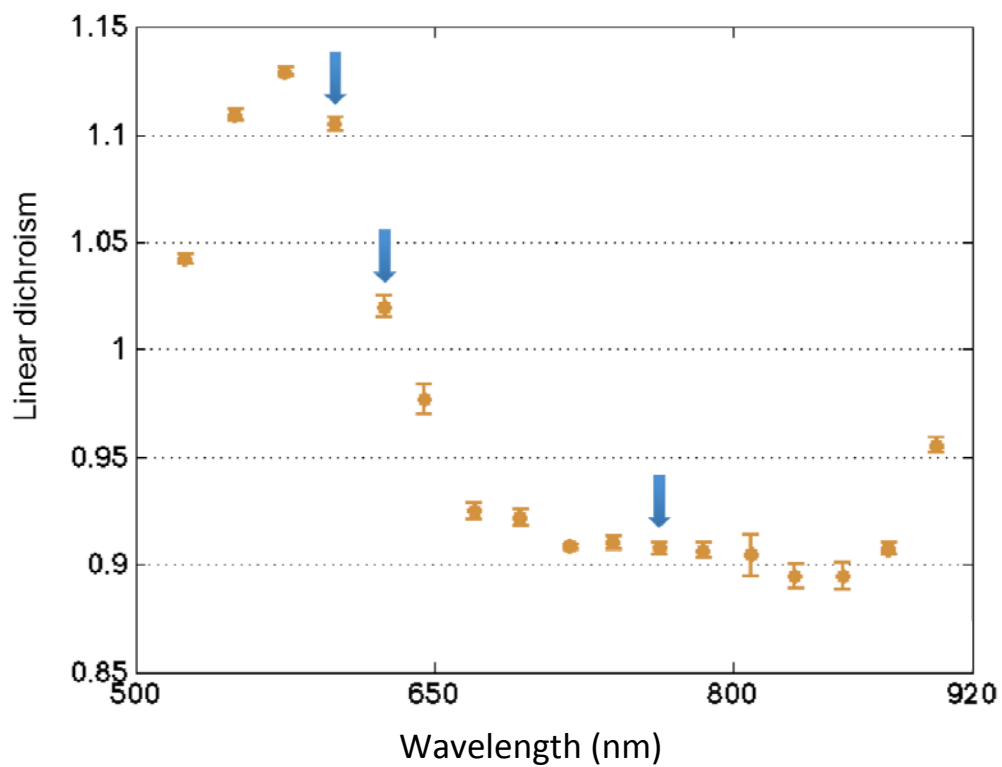


**Figure S2** Linear dichroism spectra of single nanowires as a function of excitation wavelength. Arrows indicate the wavelength where circular dichroism images were acquired.

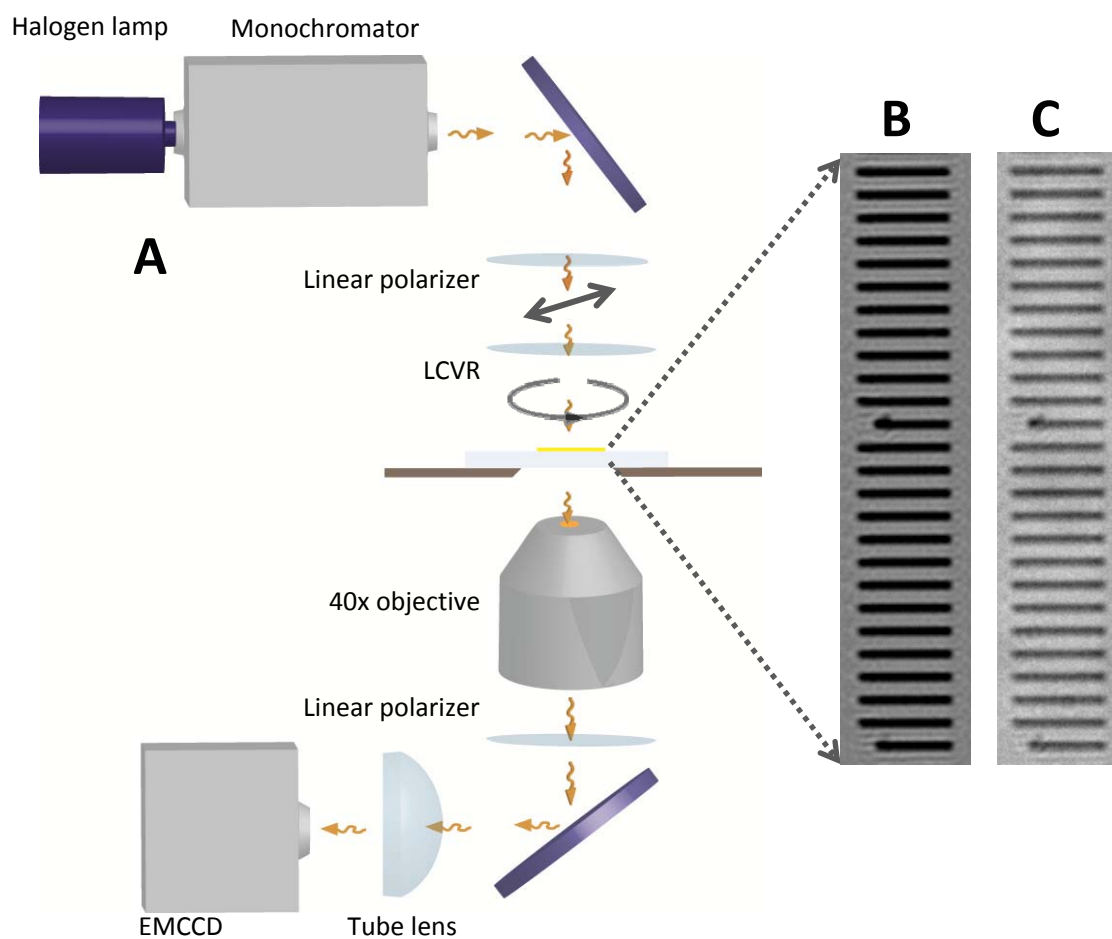


**Figure S3** Linear birefringence of single nanowires. A. Experimental apparatus; B. Map of linear birefringence at 630 nm. C. Photograph of nanowire array

$\lambda$ (nm)	Linear dichroism ( $\rho$ )	Linear birefringence ( $\beta$ )	$h$ (nm)	Global phase ( $\psi$ )	$A_0 \cdot V$ ( $\mu\text{m}^3$ )	$E_{\text{inc}}/E_{\text{sca}}$
600	1.1	0.11	360 - 720	3.0761	$1.07 \times 10^{-2}$	2.1
630	1.02	0.15	310 - 770	3.0607	$0.78 \times 10^{-2}$	1.9
760	0.91	0.1	470 - 900	3.0701	$1.18 \times 10^{-2}$	2.0

**Table S1**

Optical parameters characterizing the twisted H nanowire pairs. Linear dichroism ( $\rho$ ) and linear birefringence ( $\beta$ ) were measured on individual layers of nanowires. The gap height ( $h$ ) was determined from Newton's rings interference patterns. The global phase of scattered relative to incident light ( $\psi$ ), scattering strength ( $A_0 \cdot V$ ), and ratio of scattered to incident field strengths were used as fitting parameters.